

Interplay of Topology and Electron-Electron Interactions in Rarita-Schwinger-Weyl semimetals

Igor Boettcher^{*}

Joint Quantum Institute, University of Maryland, College Park, Maryland 20742, USA



(Received 18 July 2019; accepted 11 March 2020; published 27 March 2020)

We study, for the first time, the effects of strong short-range electron-electron interactions in generic Rarita-Schwinger-Weyl semimetals hosting spin-3/2 electrons with linear dispersion at a fourfold band crossing point. The emergence of this novel quasiparticle, which is absent in high-energy physics, has recently been confirmed experimentally in the solid state. We combine symmetry considerations and a perturbative renormalization group analysis to discern three interacting phases that are prone to emerge in the strongly correlated regime: The chiral topological semimetal breaks a \mathbb{Z}_2 symmetry and features four Weyl nodes of monopole charge +1 located at vertices of a tetrahedron in momentum space. The s -wave superconducting state opens a Majorana mass gap for the fermions and is the leading superconducting instability. The Weyl semimetal phase removes the fourfold degeneracy and creates two Weyl nodes with either equal or opposite chirality depending on the anisotropy of the band structure. We find that symmetry breaking occurs at weaker coupling if the total monopole charge remains constant across the transition.

DOI: 10.1103/PhysRevLett.124.127602

The emergence of massless fermionic quasiparticles as low-energy degrees of freedom in condensed matter systems links phenomena from high-energy physics to those of many-body systems [1]. Semimetals with the Fermi level close to a high-symmetry band crossing point provide the closest realization of the relativistic concept of a particle described by its mass and spin [2]. The exploration of such Fermi points in graphene, ultracold atoms, Dirac, Weyl, and Luttinger semimetals is on the forefront of both theoretical and experimental research [3–12].

Very recently, first experimental evidences of emergent spin-3/2 relativistic fermions with a concomitantly large topological charge have been reported in CoSi, RhSi [13–15], AlPt [16], and PdBiSe [17]. Since the standard model of particles does not feature fundamental spin-3/2 particles, although they appear as composite degrees of freedom through Δ -baryons or in conjectured extensions like supergravity [18–20], identifying their condensed matter analogs is key to studying their properties and interactions. In three-dimensional Rarita-Schwinger-Weyl (RSW) semimetals with fourfold linear band crossing points at the Fermi level, the universal low-energy $k \cdot p$ Hamiltonian reads

$$H(\mathbf{p}) = p_i(v_1 J_i + v_2 J_i^3). \quad (1)$$

Here, \mathbf{p} is the momentum measured from the crossing point, J_i are the 4×4 spin-3/2 matrices [21], $i = 1, 2, 3 = x, y, z$ with implicit summation over repeated indices, and $v_{1,2}$ are two nonuniversal material parameters. The term multiplying v_1 is rotationally invariant and

proportional to the helicity operator with eigenvalues $\pm 3/2, \pm 1/2$, making the spin-3/2 character explicit. The second term is the other scalar (linear in p_i) that can be constructed from the cubic group and reduces rotational symmetry to the rotational cubic group O for $v_2 \neq 0$, see Fig. 1. Concrete candidate materials for realizing $H(\mathbf{p})$ have been proposed at the transition to a crystalline topological insulator in antiperovskites [22,23], for many space groups and materials in Refs. [24–26], in transition metal silicides [8], and for $v_2 = 0$ through a specific tight-binding model with isotropic spin-orbit coupling on a tricolor lattice in Ref. [27]. Our model in Eq. (1) is idealized in the sense that we do not assume other band



FIG. 1. Energy dispersion of the spin-3/2 Rarita-Schwinger-Weyl fermion at a fourfold linear band crossing point. We set one of the momentum components of \mathbf{p} to zero and plot the eigenvalues of Eq. (1) versus the remaining two components for $v_2 = 0$ (left) and $v_2 = 1/3$ (right). For $v_2 = 0$ the spectrum is rotation invariant, while for generic values of v_2 , it features cubic anisotropy.

crossings at the Fermi level to be important for the interacting phases, including intervalley coupling to an RSW fermion of opposite chirality.

The impact of short-range interactions in generic RSW semimetals has not been studied so far. This is somewhat surprising when compared to the case of quadratic band touching of spin-3/2 electrons, with Eq. (1) replaced by the Luttinger Hamiltonian [28,29], where material realizations in pyrochlore iridates and half-Heuslers are rather well understood, and there exists an extensive literature on exotic interacting phases resulting from the higher spin of fermions such as spin-2 or spin-3 Cooper pairing [30–43] or octupolar magnetism [44–49]. In both RSW and Luttinger semimetals, weak short range interactions are irrelevant due to the vanishing density of states at the Fermi point, and so, the phases of interest are at strong coupling. For RSW semimetals, short-range interactions have only been investigated in the exceptional case of $\alpha = 0$ [10,11] (defined below), which is qualitatively different from $H = p_i J_i$.

In this Letter, we aim to fill this gap in the understanding of interacting RSW semimetals. Our analysis proceeds in three steps. First, we study the single-particle physics of RSW fermions to clarify the distinct relevant parameter regimes. Then, we perform an unbiased perturbative renormalization group (RG) analysis of all competing ordering channels and identify three leading strong coupling instabilities. Last, we discuss symmetries and quasi-particle spectra in the ordered phases found with the RG.

Single-particle physics.—To discuss the symmetries and topology of the RSW Hamiltonian in Eq. (1), we write

$$H(\mathbf{p}) = p_i (V_i + \alpha U_i), \quad (2)$$

with $V_i = \frac{1}{3}(-7J_i + 4J_i^3)$ and $U_i = \frac{1}{6}(13J_i - 4J_i^3)$ [23]. We have $\text{tr}(V_i V_j) = \text{tr}(U_i U_j) = 4\delta_{ij}$ and $\text{tr}(V_i U_j) = 0$. The chemical potential is at the band crossing point. We set the Fermi velocity multiplying the term $p_i V_i$ to unity so that the crossing is described by the single parameter α [50]. For $\alpha = 2$ the Hamiltonian reduces to the rotationally invariant expression $2p_i J_i$. Remarkably, the matrices V_i form a Clifford algebra,

$$\{V_i, V_j\} = 2\delta_{ij}, \quad (3)$$

and so, $H_{\alpha=0} = p_i V_i$ is Lorentz invariant with enhanced $O(2)$ symmetry. Importantly, this comprises two Weyl points of equal chirality, contrary to a Dirac Hamiltonian, which decomposes into Weyl points of opposite chirality in the massless limit.

The system is time-reversal invariant with the time-reversal operator $\mathcal{T} = \gamma_{45} \mathcal{K}$, $\mathcal{T}^2 = -1$, where \mathcal{K} is a complex conjugation and γ_{45} a Hermitean matrix defined below. For fixed \mathbf{p} , we have $\{\mathcal{T}, H(\mathbf{p})\} = 0$, and so, every eigenvalue $E(\mathbf{p})$ implies an eigenvalue $-E(\mathbf{p})$ for the

TABLE I. Normal state Chern numbers. Bands are enumerated by decreasing energy eigenvalues, see Eq. (10) with $\chi = 0$. There is a topological phase transition at $\alpha = 1$, where the total monopole charge changes. The case $\alpha = 0$ corresponds to two overlapping Weyl nodes of equal chirality.

Band	Energy	$\alpha = 0$	$0 < \alpha < 1$	$1 < \alpha$
1	$E_+(\mathbf{p})$	$C = -1$	$C = 3$	$C = 3$
2	$E_-(\mathbf{p})$	$C = -1$	$C = -5$	$C = 1$
3	$-E_-(\mathbf{p})$	$C = 1$	$C = 5$	$C = -1$
4	$-E_+(\mathbf{p})$	$C = 1$	$C = -3$	$C = -3$
Monopole charge		-2	-2	4

time-reversed eigenvector, i.e., particle-hole symmetry of the spectrum. Next, consider the Hermitean operator

$$\mathcal{W} = \frac{2}{\sqrt{3}}(J_x J_y J_z + J_z J_y J_x), \quad (4)$$

which squares to unity. We have $[V_i, \mathcal{W}] = \{U_i, \mathcal{W}\} = 0$, implying $\mathcal{W} H_\alpha \mathcal{W} = H_{-\alpha}$. Consequently, a sign change $\alpha \rightarrow -\alpha$ can be undone by $\psi \rightarrow \mathcal{W}\psi$, and so, we assume $\alpha \geq 0$.

Now, we determine the topology of the RSW point node. The eigenvectors $|\nu(\mathbf{p})\rangle$ of $H(\mathbf{p})$ for fixed \mathbf{p} comprise two positive and two negative energy bands, which we label by an index ν . For each band, we define the Berry connection $\mathbf{A}_\nu(\mathbf{p}) = -i\langle \nu(\mathbf{p}) | \nabla_{\mathbf{p}} | \nu(\mathbf{p}) \rangle$, pseudomagnetic field $\mathbf{B}_\nu(\mathbf{p}) = \nabla_{\mathbf{p}} \times \mathbf{A}_\nu(\mathbf{p})$, and Chern number $C_\nu = \oint d\vec{\Omega} \cdot \mathbf{B}_\nu(\mathbf{p})$, where the latter surface integral encloses the origin. In Table I, we present C_ν as a function of α together with the total monopole charge of the Fermi node, defined as the sum of Chern numbers of the positive energy bands. The system undergoes a topological phase transition at $\alpha = 1$, where the monopole charge changes from -2 to 4 . [Note that $H(\mathbf{p})$ features line nodes for $\alpha = 1$, which are an artefact of the linear approximation and can be eliminated by including a quadratic term.] The curious Chern numbers in the regime $0 < \alpha < 1$ do not seem to have been reported before. Note that, while RSW fermions are often associated with monopole charge 4 as in AlPt or PdBiSe, the case of charge 2 observed in CoSi or RhSi might also correspond to an RSW fermions.

Renormalization group.—The many-body physics of interacting RSW electrons is captured by the Lagrangian

$$L = \psi^\dagger [\partial_\tau + H(-i\nabla) + \bar{e}a] \psi + \frac{1}{2}(\nabla a)^2 + L_{\text{short}}, \quad (5)$$

with τ imaginary time, ψ the four-component electron spinor, a the photon that mediates long-range interactions, \bar{e} electric charge, and short-range interactions L_{short} . Because of the symmetries and dimensionality of the system, the interaction effects at low energies can be

investigated with the one-loop RG developed in Ref. [48], where Eqs. (5) and (6) have been investigated for H being the Luttinger Hamiltonian. Here, we use the same notation and adapted equations, but obviously, the physics is different due to the modified band dispersion. We refer to Ref. [48] for a very detailed introduction to the computational procedure but summarize a few central definitions in the Supplemental Material (SM) [21].

In the following, we only need to consider pointlike short-range interactions, since terms containing derivatives of the fermion field are suppressed at the Fermi point at low energies. The most general Fierz-complete form is [48]

$$L_{\text{short}} = \bar{g}_1 (\psi^\dagger \psi)^2 + \bar{g}_2 \sum_{a=1}^2 (\psi^\dagger \gamma_a \psi)^2 + \bar{g}_3 \sum_{a=3}^5 (\psi^\dagger \gamma_a \psi)^2, \quad (6)$$

where we introduce five γ matrices

$$\gamma_1 = \frac{J_x^2 - J_y^2}{\sqrt{3}}, \quad \gamma_2 = J_z^2 - \frac{5}{4} \mathbb{1}, \quad \gamma_3 = \frac{J_z J_x + J_x J_z}{\sqrt{3}}, \quad (7)$$

$$\gamma_4 = \frac{J_y J_z + J_z J_y}{\sqrt{3}}, \quad \gamma_5 = \frac{J_x J_y + J_y J_x}{\sqrt{3}}, \quad (8)$$

satisfying $\{\gamma_a, \gamma_b\} = 2\delta_{ab}$. We write $\gamma_{ab} = i\gamma_a \gamma_b$. For the RG analysis, we define dimensionless running couplings by $g_i = \Lambda^2 \bar{g}_i / (2\pi^2)$, $e^2 = \bar{e}^2 / (2\pi^2)$, with Λ the bandwidth. Although the g_i are power-counting irrelevant, they can induce ordering at strong coupling [51].

As pointed out by Isobe and Fu [23], the electric charge e gives self-energy corrections, but flows to zero. It leads to an anomalous dimension $\propto e^2$ for the fermions and, remarkably, the stable fixed points for the anisotropy are $\alpha = 0$ and $\alpha = 2.296$, whereas $\alpha = 2$ is unstable. In real materials, however, the corresponding RG flow may be stopped by finite volume effects, or suppressed by a large dielectric constant. Thus, we assume α to be a fixed number, determined by the chemical composition of the compound. Renormalization effects due to the coupling of long- and short-range interactions are equally suppressed by powers of $e^2 \rightarrow 0$ and will be neglected henceforth. (Furthermore, there is no one-loop diagram that could induce a back-reaction of $g_{1,2,3}$ onto the RG flow of e^2 [48].) The remaining RG flow equations have the form $dg_i/d \ln b = -2g_i + C_{ijk}(\alpha)g_j g_k$, where $C_{ijk}(\alpha)$ are coefficients that result from integrating out fluctuations of RSW electrons in a momentum shell $\Lambda \geq p \geq \Lambda/b$. The coefficients parametrically depend on α through the anisotropic fermion dispersion.

We search for quantum critical points, which are fixed points of the RG flow where exactly one linear combination of g_1, g_2, g_3 is a relevant direction. At every fixed point, we

determine the scaling dimension of the ten fermion bilinears $\psi^\dagger M \psi^{(*)}$ allowed by symmetry through coupling a term $h \psi^\dagger M \psi^{(*)}$ to the Lagrangian and determining the flow $\dot{h} = (1 + \eta)h$. The bilinear with the largest susceptibility η condenses at the associated quantum phase transition [21]. Both fixed points and susceptibilities depend on α . We identify three distinct quantum critical points (labeled W, SC, V), which are related to the following order parameters: (1) chiral topological semimetal (W): $\chi = \langle \psi^\dagger \mathcal{W} \psi \rangle \neq 0$. (2) s -wave superconductor (SC): $\phi = \langle \psi^\dagger \gamma_4 \psi^{*} \rangle \neq 0$. (3) Weyl semimetal (V): $m_i = \langle \psi^\dagger V_i \psi \rangle \neq 0$. The identification of these three leading instabilities in interacting RSW semimetals from an unbiased RG analysis constitutes the first major result of this Letter.

The three fixed points have the following properties, which are visualized in Fig. 2: The large critical couplings $g_{i,c} \sim 1$ are due to the vanishing density of states at the Fermi point. Whereas SC and V exist for every α , W only exists for $\alpha > 0$. W : Here, the ratio of critical couplings is $g_1 = -g_2 = g_3 = 2g_* > 0$ for all α , implying the system

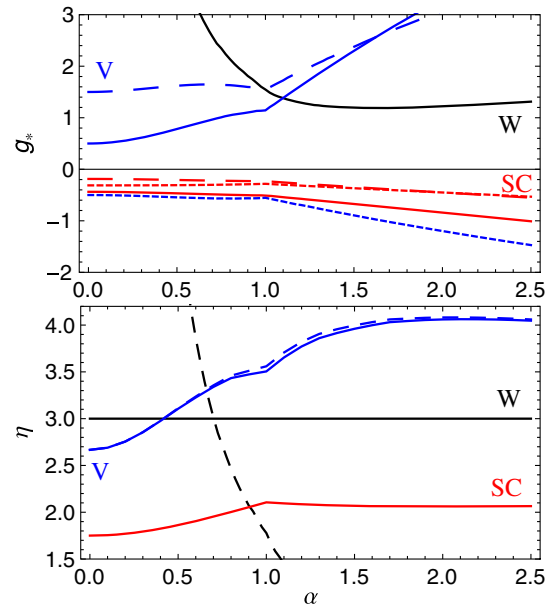


FIG. 2. Renormalization group fixed points. Upper panel: Couplings g_1, g_2, g_3 (solid, dashed, dotted lines) at the fixed points W (black), SC (red), and V (blue). At W , we have $g_1 = -g_2 = g_3$, and so, we only show the first coupling. Lower panel: Susceptibility exponent η of the order parameter at the fixed points. At W , we have $\eta = 3$ for $\langle \psi^\dagger \mathcal{W} \psi \rangle$ for all $\alpha > 0$ (solid black line). This is the dominant divergence for $\alpha > 0.7$, while for $\alpha < 0.7$ the order parameter $N_i(\alpha) = \langle \psi^\dagger [V_i + \kappa(\alpha)U_i] \psi \rangle$ with $\kappa(\alpha) \gg 1$ has the largest susceptibility (dashed black line). At SC , the most divergent channel is the s -wave superconductor (red). At V , $N_i(\alpha)$ has the largest susceptibility exponent (dashed blue line). Since, here, $\kappa(\alpha)$ is generically very small, we can neglect it and only consider the approximate order parameter $\langle \psi^\dagger V_i \psi \rangle$ (solid blue line).

flows to the fixed point Lagrangian (9). The susceptibility exponent of χ is exactly given by the spatial dimension, $\eta_{\mathcal{W}} = d = 3$, which comprises the leading instability in the regime $\alpha \geq 0.70$. For $\alpha < 0.7$, the order parameter has large overlap with $\langle \psi^\dagger U_i \psi \rangle$ instead, but we will not further discuss it in this Letter. SC: This is a superconducting quantum critical point corresponding to a condensation of ϕ , which acts as a Majorana mass term for the fermions, see Eq. (12). V: The fixed point V corresponds to a condensation of m_i . More precisely, the order parameter receives a small admixture of U_i according to $\langle \psi^\dagger [V_i + \kappa(\alpha)U_i] \psi \rangle$. However, $\kappa = 0$ for $\alpha = 0$ and $\kappa(\alpha) < 5\%$ in general, so we neglect this effect for the discussion here but plot the function $\kappa(\alpha)$ for completeness in the SM [21].

Chiral topological semimetal.—Now, we characterize the properties of the chiral topological semimetal phase, which is the second major result of this Letter. We verified above that the system at W , after fine-tuning one coupling, is attracted to the fixed point Lagrangian

$$L_\star = \psi^\dagger (\partial_\tau + H) \psi - \bar{g}_\star (\psi^\dagger \mathcal{W} \psi)^2, \quad (9)$$

with $\bar{g}_\star > 0$. In the mean field approximation, we replace $-\bar{g}_\star (\psi^\dagger \mathcal{W} \psi)^2 \rightarrow \chi (\psi^\dagger \mathcal{W} \psi)$ and arrive at effectively non-interacting fermionic quasiparticles described by the Hamiltonian $H_{\text{mf}}(\mathbf{p}) = H(\mathbf{p}) + \chi \mathcal{W}$. Note that \mathcal{W} is invariant under the rotational or chiral tetrahedral group T only [21]. The term $\chi \mathcal{W}$ breaks time-reversal symmetry, but preserves particle-hole symmetry of the energy spectrum. The positive eigenvalues of $H_{\text{mf}}(\mathbf{p})$ are

$$E_\pm(\mathbf{p}) = \left\{ \chi^2 + (1 + \alpha^2)p^2 \pm \left[4\chi^2 p^2 + \alpha^2 \left(4p^4 - 3(4 - \alpha^2) \sum_{i < j} p_i^2 p_j^2 + 12\sqrt{3}\chi p_1 p_2 p_3 \right) \right]^{1/2} \right\}^{1/2}. \quad (10)$$

We have $E_+(\mathbf{p}) > 0$. The zeros of $E_-(\mathbf{p})$ are located at the four vertices of a tetrahedron according to $\mathbf{p}_n = (\chi/\sqrt{3})\mathbf{e}_n$ with

$$\begin{aligned} \mathbf{e}_1 &= \begin{pmatrix} 1 \\ 1 \\ 1 \end{pmatrix}, & \mathbf{e}_2 &= \begin{pmatrix} -1 \\ -1 \\ 1 \end{pmatrix}, \\ \mathbf{e}_3 &= \begin{pmatrix} -1 \\ 1 \\ -1 \end{pmatrix}, & \mathbf{e}_4 &= \begin{pmatrix} 1 \\ -1 \\ -1 \end{pmatrix}. \end{aligned} \quad (11)$$

The α dependence of the nodes is implicit, through χ , which is the solution of an α -dependent gap equation. The sign of the order parameter χ gives the configuration of Weyl nodes a handedness so that it cannot be rotated into its mirror

image with the z component reversed in sign, thereby breaking a \mathbb{Z}_2 symmetry.

To clarify the nature of the gapless quasiparticles at the nodal points, we compute $\mathbf{B}_\nu(\mathbf{p})$ for the two bands with energy $\pm E_-(\mathbf{p})$ and determine the Chern number C from the surface integral surrounding \mathbf{p}_n in momentum space. At each vertex of the tetrahedron, the positive energy band has $C = 1$ and the negative energy band has $C = -1$, so the total monopole charge is 4. Thus, for $\alpha > 1$ the phase transition is such that the normal state charge of $+4$ is distributed onto four unit charges $+1$. For $0 < \alpha < 1$, on the other hand, symmetry breaking implies a topological phase transition which changes the total monopole charge.

The effective Weyl Hamiltonian that describes excitations with momentum $\mathbf{p} = \mathbf{p}_n + \delta\mathbf{p}$ close to the nodal points can be obtained from projecting onto the subspace spanned by the zero modes $|0_n\rangle, |0'_n\rangle$ of $H(\mathbf{p}_n)$, yielding $H_0^{(n)}(\delta\mathbf{p}) = v_{ij}^{(n)} \delta p_i \sigma_j$, which constitutes type-I Weyl nodes. The energy close to the nodal point reads $E^{(n)}(\delta\mathbf{p}) = \pm \sqrt{\delta p_i (v^{(n)} v^{(n)T})_{ij} \delta p_j}$ and the monopole charge of each Weyl node is consistently given by $\text{sgn}[\det(v^{(n)})] = \text{sgn}(\alpha^2) = 1$. The matrices $v^{(n)}$ are displayed in the SM [21].

Dirac, Majorana, and Weyl mass terms.—Identifying fermion bilinears that open a full gap (“mass terms”) is an important step in finding energetically favorable ordering patterns for any new single-particle Hamiltonian and, as such, complements the perturbative RG analysis. In the following, we discuss three canonical mass terms in the system: those of Dirac-, Majorana-, and Weyl-types. First, we derive the negative result that the Hamiltonian $H = p_i V_i$ for $\alpha = 0$ does not permit a Dirac mass term, which would be a fourth matrix M that anticommutes with all V_i . Indeed, the 4×4 Clifford algebra $\{A_n, A_m\} = 2\delta_{nm}\mathbb{1}$ allows for two inequivalent representations: One reads $A_i = \mathbb{1}_2 \otimes \sigma_i$, which is a reducible representation where no fourth anticommuting matrix exists. The second solution is $A_1 = \sigma_1 \otimes \mathbb{1}_2, A_2 = \sigma_3 \otimes \mathbb{1}_2, A_3 = \sigma_2 \otimes \sigma_2, A_4 = \sigma_2 \otimes \sigma_1, A_5 = \sigma_2 \otimes \sigma_3$, and so, after choosing three matrices to construct a Hamiltonian $p_i A_i$, there are two left to form mass terms. With a suitable basis change, one easily sees that $V_i \sim \mathbb{1}_2 \otimes \sigma_i$ in RSW semimetals [21], which is of the first type, implying the leading (particle-number conserving) instability for $\alpha = 0$ to have nodes. Note that the Hamiltonian considered in Ref. [11] reads $p_i(\mathbb{1}_2 \otimes \sigma_i + \beta \sigma_i \otimes \mathbb{1}_2)$, with β a real parameter, and so, only for $\beta = 0$ has overlap with the RSW Hamiltonian.

In the s -wave superconducting phase, the system develops a Majorana mass term. The corresponding effective Lagrangian reads [30]

$$L_{\text{sc}} = \psi^\dagger (\partial_\tau + H) \psi - g_s (\psi^\dagger \gamma_{45} \psi^*) (\psi^T \gamma_{45} \psi), \quad (12)$$

with superconducting gap $\Delta \propto \langle \psi^\dagger \gamma_{45} \psi^* \rangle$ and $g_s > 0$. Recall that a Majorana mass term for two-component fermions reads $\psi^\dagger \sigma_2 \psi^*$. The energies of quasiparticles are $E(\mathbf{p}) = \pm \sqrt{E_0(\mathbf{p})^2 + |\Delta|^2}$, with $E_0(\mathbf{p})$ the spectrum of H . The suppression of low-energy excitations explains the superiority of the s -wave superconductor among all particle-number nonconserving orders in the perturbative RG computation.

Eventually, consider adding a Weyl mass $m_i V_i$ to the Hamiltonian. As is well known, for $\alpha = 0$, this merely shifts the position of the Weyl nodes, but for $\alpha > 0$, the effect is far more intriguing. Assume the minimal free energy is obtained for a state with residual SO(2) symmetry, and so, $\vec{m} = (0, 0, m)$. The nodes of the mean-field Hamiltonian $H_V(\mathbf{p}) = H(\mathbf{p}) + mV_3$ are located at

$$\mathbf{p}_a = \frac{-m}{1+\alpha}(0, 0, 1)^T, \quad \mathbf{p}_b = \frac{-m}{1-\alpha}(0, 0, 1)^T, \quad (13)$$

assuming $\alpha \neq 1$. These momenta again correspond to type-I Weyl nodes [21]. Remarkably, the monopole charge associated to each of the two Weyl nodes is given by

$$q_a = -1, \quad q_b = \text{sgn}(\alpha - 1). \quad (14)$$

Consequently, there is a topological phase transition in the broken phase when crossing $\alpha = 1$, with the total monopole charge being -2 for $\alpha < 1$ and 0 for $\alpha > 1$. For $\alpha < 1$, the monopole charge remains constant upon condensation of $m \neq 0$. The identification of this Weyl semimetal phase constitutes the third major result of this Letter.

Conclusion.—Our analysis reveals an intriguing interplay between topology and interactions. First, the critical couplings of W and V are smaller in those regimes where the total monopole charge does not change across the transition ($\alpha > 1$ for W and $\alpha < 1$ for V), and so, no topological phase transition occurs besides the symmetry breaking. Second, the critical coupling for W has no kink at $\alpha = 1$ and the scaling dimension of the order parameter is independent at α , indicating a topological nature of the ordering. The rearranged monopole structure in the ordered phases can be revealed experimentally through surface state spectroscopy [7,8] or optical response measurements [11,52]. It will be exciting to study the interplay of a pair of RSW fermions with opposite monopole charges, similar to the interplay of Weyl nodes in Weyl semimetals [53].

I gratefully acknowledge collaboration with Michael Scherer in an early stage of this work. I thank Igor Herbut for inspiring discussions and for bringing to my attention the relation of these findings to the representation theory of Clifford algebras. I thank Fabian von Rohr for insightful comments. This work was supported by Department of Energy (DOE) Basic Energy Sciences Materials and Chemical Sciences Research for Quantum Information Science program, National Science Foundation (NSF) Ideas Lab on Quantum Computing,

DOE Advanced Scientific Computing Research Quantum Testbed Pathfinder Program, Army Research Office Multidisciplinary University Research Initiative, Army Research Laboratory Center for Distributed Quantum Information, and NSF Physics Frontier Center at Joint Quantum Institute.

*iboettch@umd.edu

- [1] G. E. Volovik, *The Universe in a Helium Droplet* (Oxford University Press, New York, 2003).
- [2] S. Weinberg, *The Quantum Theory of Fields Volume I: Foundations* (Cambridge University Press, Cambridge, England, 2005).
- [3] A. K. Geim and K. S. Novoselov, *Nat. Mater.* **6**, 183 (2007).
- [4] M. Z. Hasan and C. L. Kane, *Rev. Mod. Phys.* **82**, 3045 (2010).
- [5] X.-L. Qi and S.-C. Zhang, *Rev. Mod. Phys.* **83**, 1057 (2011).
- [6] L. Huang, Z. Meng, P. Wang, P. Peng, S.-L. Zhang, L. Chen, D. Li, Q. Zhou, and J. Zhang, *Nat. Phys.* **12**, 540 (2016).
- [7] G. Chang, S.-Y. Xu, B. J. Wieder, D. S. Sanchez, S.-M. Huang, I. Belopolski, T.-R. Chang, S. Zhang, A. Bansil, H. Lin, and M. Z. Hasan, *Phys. Rev. Lett.* **119**, 206401 (2017).
- [8] P. Tang, Q. Zhou, and S.-C. Zhang, *Phys. Rev. Lett.* **119**, 206402 (2017).
- [9] N. P. Armitage, E. J. Mele, and A. Vishwanath, *Rev. Mod. Phys.* **90**, 015001 (2018).
- [10] S. E. Han and E.-G. Moon, *Phys. Rev. B* **97**, 241101(R) (2018).
- [11] B. Roy, M. P. Kennett, K. Yang, and V. Jurićić, *Phys. Rev. Lett.* **121**, 157602 (2018).
- [12] H. Gao, J. W. Venderbos, Y. Kim, and A. M. Rappe, *Annu. Rev. Mater. Res.* **49**, 153 (2019).
- [13] D. Takane, Z. Wang, S. Souma, K. Nakayama, T. Nakamura, H. Oinuma, Y. Nakata, H. Iwasawa, C. Cacho, T. Kim, K. Horiba, H. Kumigashira, T. Takahashi, Y. Ando, and T. Sato, *Phys. Rev. Lett.* **122**, 076402 (2019).
- [14] Z. Rao *et al.*, *Nature (London)* **567**, 496 (2019).
- [15] D. S. Sanchez, I. Belopolski, T. A. Cochran, X. Xu, J. Yin, G. Chang, W. Xie, K. Manna, V. Süß, C.-Y. Huang, N. Alidoust, D. Multer, S. S. Zhang, N. Shumiya, X. Wang, G.-Q. Wang, T.-R. Chang, C. Felser, S.-Y. Xu, and M. Z. Hasan, *Nature (London)* **567**, 500 (2019).
- [16] N. B. M. Schröter, D. Pei, M. G. Vergniory, Y. Sun, K. Manna, F. de Juan, J. A. Krieger, V. Süß, M. Schmidt, and P. Dudin, *Nat. Phys.* **15**, 759 (2019).
- [17] B. Q. Lv, Z.-L. Feng, J.-Z. Zhao, N. F. Q. Yuan, A. Zong, K. F. Luo, R. Yu, Y.-B. Huang, V. N. Strocov, A. Chikina, A. A. Soluyanov, N. Gedik, Y.-G. Shi, T. Qian, and H. Ding, *Phys. Rev. B* **99**, 241104(R) (2019).
- [18] W. Rarita and J. Schwinger, *Phys. Rev.* **60**, 61 (1941).
- [19] D. Z. Freedman, P. van Nieuwenhuizen, and S. Ferrara, *Phys. Rev. D* **13**, 3214 (1976).
- [20] L. Liang and Y. Yu, *Phys. Rev. B* **93**, 045113 (2016).
- [21] See Supplemental Material at <http://link.aps.org/supplemental/10.1103/PhysRevLett.124.127602> for the definition of spin-3/2 matrices, effective Weyl Hamiltonians, details of the renormalization group analysis, and a brief summary of cubic symmetry group.

- [22] T. H. Hsieh, J. Liu, and L. Fu, *Phys. Rev. B* **90**, 081112(R) (2014).
- [23] H. Isobe and L. Fu, *Phys. Rev. B* **93**, 241113(R) (2016).
- [24] B. Bradlyn, J. Cano, Z. Wang, M. G. Vergniory, C. Felser, R. J. Cava, and B. A. Bernevig, *Science* **353**, aaf5037 (2016).
- [25] G. Chang, B. J. Wieder, F. Schindler, D. S. Sanchez, I. Belopolski, S.-M. Huang, B. Singh, D. Wu, T.-R. Chang, T. Neupert, S.-Y. Xu, H. Lin, and M. Z. Hasan, *Nat. Mater.* **17**, 978 (2018).
- [26] J. Cano, B. Bradlyn, and M. G. Vergniory, *APL Mater.* **7**, 101125 (2019).
- [27] M. Ezawa, *Phys. Rev. B* **94**, 195205 (2016).
- [28] E.-G. Moon, C. Xu, Y. B. Kim, and L. Balents, *Phys. Rev. Lett.* **111**, 206401 (2013).
- [29] I. F. Herbut and L. Janssen, *Phys. Rev. Lett.* **113**, 106401 (2014).
- [30] I. Boettcher and I. F. Herbut, *Phys. Rev. B* **93**, 205138 (2016).
- [31] P. M. R. Brydon, L. Wang, M. Weinert, and D. F. Agterberg, *Phys. Rev. Lett.* **116**, 177001 (2016).
- [32] D. F. Agterberg, P. M. R. Brydon, and C. Timm, *Phys. Rev. Lett.* **118**, 127001 (2017).
- [33] S. A. A. Ghorashi, S. Davis, and M. S. Foster, *Phys. Rev. B* **95**, 144503 (2017).
- [34] W. Yang, T. Xiang, and C. Wu, *Phys. Rev. B* **96**, 144514 (2017).
- [35] L. Savary, J. Ruhman, J. W. F. Venderbos, L. Fu, and P. A. Lee, *Phys. Rev. B* **96**, 214514 (2017).
- [36] I. Boettcher and I. F. Herbut, *Phys. Rev. Lett.* **120**, 057002 (2018).
- [37] J. W. F. Venderbos, L. Savary, J. Ruhman, P. A. Lee, and L. Fu, *Phys. Rev. X* **8**, 011029 (2018).
- [38] H. Kim, K. Wang, Y. Nakajima, R. Hu, S. Ziemak, P. Syers, L. Wang, H. Hodovanets, J. D. Denlinger, P. M. R. Brydon, D. F. Agterberg, M. A. Tanatar, R. Prozorov, and J. Paglione, *Sci. Adv.* **4**, eaao4513 (2018).
- [39] S. A. A. Ghorashi, P. Hosur, and C.-S. Ting, *Phys. Rev. B* **97**, 205402 (2018).
- [40] I. Mandal, *Ann. Phys. (Amsterdam)* **392**, 179 (2018).
- [41] J. Yu and C.-X. Liu, *Phys. Rev. B* **98**, 104514 (2018).
- [42] B. Roy, S. A. A. Ghorashi, M. S. Foster, and A. H. Nevidomskyy, *Phys. Rev. B* **99**, 054505 (2019).
- [43] G. B. Sim, A. Mishra, M. J. Park, Y. B. Kim, G. Y. Cho, and S. B. Lee, *Phys. Rev. B* **100**, 064509 (2019).
- [44] L. Savary, E.-G. Moon, and L. Balents, *Phys. Rev. X* **4**, 041027 (2014).
- [45] W. Witczak-Krempa, G. Chen, Y. B. Kim, and L. Balents, *Annu. Rev. Condens. Matter Phys.* **5**, 57 (2014).
- [46] J. M. Murray, O. Vafek, and L. Balents, *Phys. Rev. B* **92**, 035137 (2015).
- [47] P. Goswami, B. Roy, and S. D. Sarma, *Phys. Rev. B* **95**, 085120 (2017).
- [48] I. Boettcher and I. F. Herbut, *Phys. Rev. B* **95**, 075149 (2017).
- [49] X.-P. Yao and G. Chen, *Phys. Rev. X* **8**, 041039 (2018).
- [50] In the notation of Eq. (S121) of the Supplemental Material of Ref. [24], we have $\alpha = (a - b)/(a + b)$.
- [51] I. Herbut, *A Modern Approach to Critical Phenomena* (Cambridge University Press, Cambridge, England, 2007).
- [52] I. Boettcher, *Phys. Rev. B* **99**, 125146 (2019).
- [53] J. Maciejko and R. Nandkishore, *Phys. Rev. B* **90**, 035126 (2014).